Design and Pressure Loss Reduction in the Hydrogen Flow Heat Exchanger with Tube Bundles

By
Ahmad Sleiti, Ph.D.
asleiti@mail.ucf.edu

College of Engineering and Computer Science
University of Central Florida
Orlando, FL 32816-2450

ABSTRACT

Pressure drop reduction in the hydrogen gas that enters a heat exchanger with tube bundles coaxially and guided radially for cooling purposes is investigated. Due to the drastic change in the flow direction and its inherently three-dimensional nature, the resultant pressure loss constitutes a long-term cost for the operation of the overall system. To optimize the design, a one-dimensional model of the fluid flow is established to calculate the pressure drop across the Heat Exchanger (HE) using existing correlations. The calculations showed that the proposed enhanced design can reduce the pressure loss across the cooler by about 12% for the studied range of flow rate. Then, computational fluid dynamics (CFD) tools were used to investigate enhanced designs. The existing geometry of the cooler as well as the test rig geometry from which experimental data were available were used to validate the computational results. Two approaches have been investigated to model the tube bundle finned tubes: porous media approximation and effective diameter concept. The advantage of the latter approach over the former is that the path of the fluid and the detailed history of the pressure and velocity across the tube bundle can be tracked precisely. Hence the effective diameter approach was used to model the flow across the tube bundle for six different designs. The final enhanced design showed a reduction in total mass weighted average pressure drop of 15% compared to existing design at the desired flow rate.

Keywords: Heat Exchanger, Tube Bundle, Pressure Drop, CFD

Nomenclature:
d_h = hydraulic diameter (m)
g = acceleration of gravity (m/s^2)
h = elevation (m)
l = length of duct or pipe (m)

p = pressure in fluid (Pa (N/m^2))
p_{loss} = pressure loss (Pa (N/m^2))
ρ = density of the fluid (kg/m^3)
v = flow velocity (m/s)
f = friction factor

1. INTRODUCTION AND BACKGROUND

The performance of electric generators depends on stress, rotor vibrations and thermal behavior. Once the physical size of the machine has been limited by the mechanical constraints, the only remaining way by which the power output may be increased is via increases in the electrical and magnetic loadings in the stator and rotor of the machine. The implied consequential increase in the absolute level of general inefficiencies within the machine necessitates a reliable cooling system to be incorporated into the fundamental design concept. This is to ensure that the thermal losses are dissipated at temperature levels compatible with an acceptable lifespan of the electrical materials used in generator construction.

For decades researchers have investigated various aspects of cooling in generators in order to understand flow and heat transfer characteristics in these machines so that more optimal and efficient designs can be achieved. The flow and heat transfer in grooved annuli commonly used in electric rotating machinery have been studied by many researchers [1-3]. Research on heat transfer and fluid flow mainly in large electrical machines can be found in [4]. The author [5-9] has studied several configurations with higher rotation numbers and higher wall heat flux.

In Hydrogen cooled large electric generators, hydrogen gas at 414 to 517 kPa is circulated through the generator and cooled by coolers. Hydrogen gas is used because of its high thermal diffusivity (1.5 cm^2/sec, compared with 0.2 cm^2/sec of air at STP) that would allow more compact geometry and lower flow rates (i.e., lower costs) and lower power required to blow the gas through the generator and cooler (greater generator efficiency) respectively.

Because of the inherent cylindrical geometry of generators, the use of space is greatly enhanced by using a circular water cooler. The hydrogen gas, after leaving the generator is turned around to flow axially in the space between generator housing and the water cooler. The gas will then have to enter the water cooler in the radially inward direction to be cooled before entering the generator assembly, where heat is generated both by friction of bearing and by the generator due to electrical and magnetic dissipation. In summary, hydrogen is blown in a closed loop through the generator components and then through the cooler removing the heat and returned to the generator.

The pressure loss for a flow rate of nearly 90 m^3/sec (average velocity 20 m/s or 45 MPH) in the cross section is expected to be large. However, existing data for similar flow configuration is very limited and focused predominantly on pin fins fixed at the circumference of a cylindrical straight tube that are not even close to the geometry in question. The limited knowledge is the primary obstacle to future improvement on the generator efficiency. As a first step toward generating necessary data for design consideration for pressure reduction, a computational fluid dynamics (CFD) study was performed and reported in this paper. The objectives of this study are:

(1) To investigate, using current state-of-the-art CFD tools, the pressure drop of the existing geometry of the cooler and to compare to experimental pressure drop measurements performed previously.

(2) To investigate several designs that would provide reduction in pressure drop and to determine the best design.

The tasks to be completed are:

- establish a one-dimensional *analytical* model of the fluid flow,
- establish a two-dimensional axisymmetric computational model for current geometry as well as for experimental test rig geometry,
- perform benchmark calculations to determine the pressure drop for the current geometry and for geometry used in the test rig at specified flow rates and validate the computational approach,
- propose and investigate enhanced designs and compare to current design, and determine the final design that would provide the maximum reduction in pressure drop.

2. GEOMETRY OF THE HEAT EXCHANGER AND THE TEST RIG

Figure 1 gives geometry and dimensions for the flow model. Figure 2 provides geometry for experimentally tested flow domain. The tube bundle contains four sections of tubes each section contains 68 finned tubes, which makes the total number of finned tubes in the bundle 272 tubes. The diameter of tubes is 20mm placed at 34.5mm spacing. The fins are made of copper of 0.25 mm thickness and of diameter = 34mm with fin pitch =3.5mm. The experimental pressure drop measurements will be used to validate the computational flow model and the effective diameter concept of the tubes in the bundle.

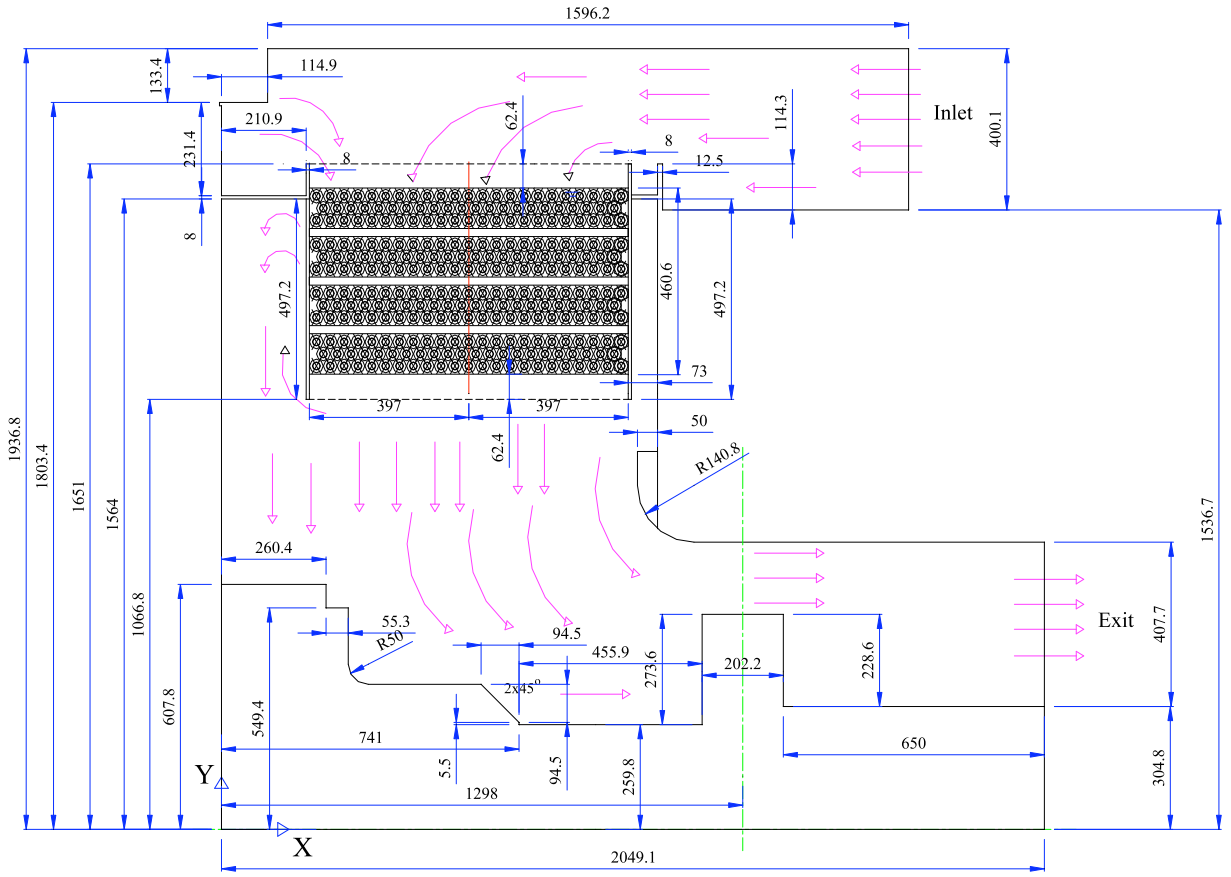

Figure 1: Geometry and flow domain for existing design (Geometry #1). Dimensions are in mm.

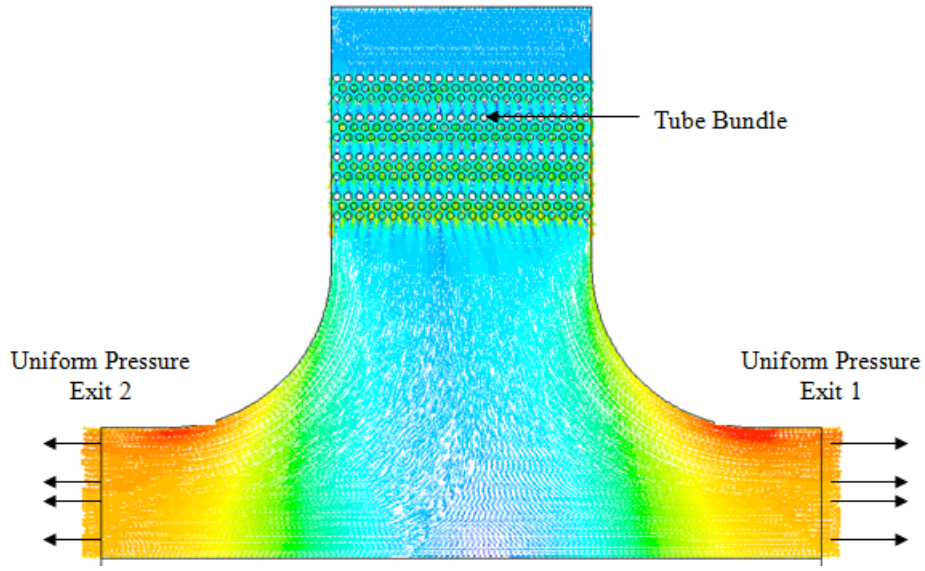

Figure 2: Geometry and flow domain for experimentally tested geometry. (Geometry #0)

3. PRESSURE LOSS CALCULATIONS

The pressure drop is calculated analytically based on major and minor pressure losses and the corresponding friction factors.

3.1 Pressure loss calculation in the entrance region

The pressure loss in the entrance of the cooler is divided into major loss due to friction and minor loss due to change of velocity in bends, turns, etc. :

3.1.1 Major loss - pressure loss - due to friction

According to the Energy Equation for a fluid the total energy can be summarized as elevation energy, velocity energy and pressure energy. The Energy Equation can be expressed as [10]:

$$p_1 + \rho\, v_1^2 / 2 + \rho\, g\, h_1 = p_2 + \rho\, v_2^2 / 2 + \rho\, g\, h_2 + p_{loss} \qquad (1)$$

where
p = pressure in fluid (Pa (N/m^2), psi (lb/ft^2))
p_{loss} = pressure loss (Pa (N/m^2), psi (lb/ft^2))
ρ = density of the fluid (kg/m^3, $slugs/ft^3$)
v = flow velocity (m/s, ft/s)
g = acceleration of gravity (m/s^2, ft/s^2)
h = elevation (m, ft)

The pressure loss in pipes and tubes depends on the flow velocity, pipe or duct length, pipe or duct diameter, and a friction factor based on the roughness of the pipe or duct, and whether the flow is turbulent or laminar - the Reynolds Number of the flow. The pressure loss in a tube or duct due to friction, major loss, can be expressed as:

$$p_{loss} = f\,(l / d_h)\,(\rho\, v^2 / 2) \qquad (2)$$

where
p_{loss} = pressure loss (Pa, N/m^2)
f = friction factor
l = length of duct or pipe (m)
d_h = hydraulic diameter (m)

Equation (2) is also called the Darcy-Weisbach Equation and is valid for fully developed, steady, incompressible flow, see [10].

The friction coefficient, f depends on the flow - if it is laminar, transient or turbulent - and the roughness of the tube or duct. For turbulent flow the friction coefficient depends on the Reynolds Number and the roughness of the duct or pipe wall. On functional form this can be expressed as:

$$f = \mathrm{f}(\mathrm{Re}, \varepsilon / d_h) \qquad (3)$$

where
ε = relative roughness of tube or duct wall (mm)
ε / d_h = the roughness ratio

The friction coefficient - λ - can be calculated by the Colebrooke Equation:

$$1 / f^{1/2} = -2{,}0 \log_{10} [\, (2.51 / (\mathrm{Re}\, f^{1/2})) + (\varepsilon / d_h) / 3.72 \,] \qquad (4)$$

3.1.2 Minor Loss

Pressure drops and minor loss in components correlates with the dynamic pressure and the minor loss can be expressed as:

$$p_{loss} = \xi\, 1/2\, \rho\, v^2 \qquad (5)$$

where
ξ = minor loss coefficient
p_{loss} = pressure loss (Pa (N/m^2))
v = flow velocity (m/s)

The minor losses in components depend primarily on the geometrical construction of the component and the impact the construction has on the fluid flow due to change in velocity and cross flow fluid accelerations. The fluid properties - in general expressed with the Reynolds number - also impact the minor loss. Table 1 provides commonly used in open literature minor loss coefficients for air ducts.

Table 1: Minor loss coefficients for different components common in air ducts:

Component or Fitting	**Minor Loss**

	Coefficient, ξ
90^o bend, sharp	1.3
90^o bend, with vanes	0.7
90^o bend, rounded radius/diameter duct <1	0.5
90^o bend, rounded radius/diameter duct >1	0.25
Enlargement, abrupt (due to speed before reduction) (v_1= velocity before enlargement and v_2 = velocity after enlargement)	$(1 - v_2 / v_1)^2$
Enlargement, tapered angle < 8^o (due to speed before reduction) (v_1= velocity before enlargement and v_2 = velocity after enlargement)	$0.15 (1 - v_2 / v_1)^2$

3.2 Pressure loss calculation in high-finned tube bank

Most of the correlations for pressure drop across banks of finned tubes in open literature are subject to great uncertainty, [11], [12]. Robinson and Briggs [13] Correlation is one of the better correlations as discussed in [13] and is given as follows:

$$f_r = 9.47\left(\frac{d_r \vartheta_{air} V_{\max}}{\mu_{air}}\right)^{-0.32}\left(\frac{P_t}{d_r}\right)^{-0.93} \qquad (6)$$

where fr is the friction factor and Pt is the transverse pitch between adjacent tubes in the same row. The friction factor is defined as

$$f_r = \frac{\Delta p_{air} g_c}{2n\vartheta_{air} V_{\max}^2} \qquad (7)$$

where ΔP_{air} is the pressure drop across the tube bank and n is the number of tubes in rows in the bank. The correlation represents data for tube banks with root diameters from 0.734 to 1.61 in., fin diameters from 1.561 in. to 2.750 in., and pitches from 1.687 to 4.5 in. Theses parameters fall within the range of parameters studied in this paper, which makes Robinson and Briggs [13] Correlation most suitable correlation to be used for validation purposes.

3.3 One dimensional analytical results of pressure loss

3.3.1 Pressure loss for existing design

The existing design contains sharp turns and edges as shown in Figure 3. Pressure loss results are given in Tables 2 and 3 for flow rates of Q_1 and Q_2, respectively.

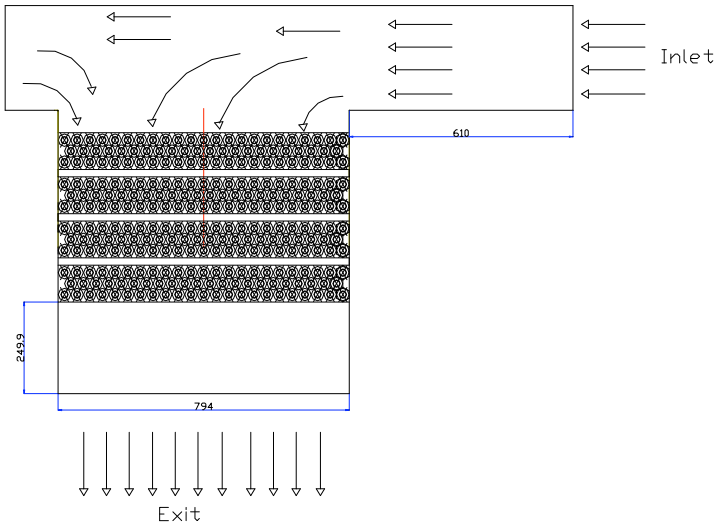

Figure 3: Analytical flow domain for existing design

Table 2: Pressure loss for Case-1: Q_1=64.2614 m^3/s – existing design

Losses	**Loss Coefficient**	**Pressure Drop**
	[ ]	[Pa]
(1) Major Loss-Friction	0.0175	7.50
(2) Minor Loss	1.5 and 3.89	231.5
(3) Loss in Bank of Tubes	0.2659	902.5
Total Loss		**1141.5**

Table 3: Pressure loss for Case-2: Q_2=67.1936 m^3/s – existing design

Losses	**Loss Coefficient**	**Pressure Drop**
	[ ]	[Pa]
(1) Major Loss-Friction	0.0175	8.00
(2) Minor Loss	0.5 and 1.3	253
(3) Loss in Bank of Tubes	0.2659	975.5
Total Loss		**1236.5**

3.3.2 Pressure loss for proposed enhanced design

An enhanced design is proposed by introducing smoothly rounded 90 deg bends and guide vanes to replace sharp turns and edges as shown in Figure 4. Pressure loss results for enhanced design are given in Tables 4 and 5 for flow rates of Q_1 and Q_2, respectively.

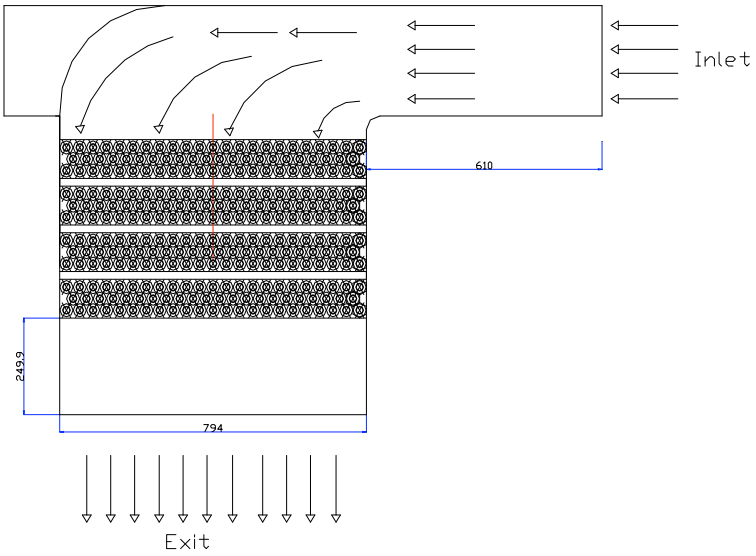

Figure 4: Analytical flow domain for enhanced design

Table 4: Pressure loss for Case-1: Q_1=64.2614 m^3/s – enhanced design

Losses	**Loss Coefficient**	**Pressure Drop**
	[ ]	[Pa]
(1) Major Loss-Friction	0.0175	7.50
(2) Minor Loss	0.5 and 1.3	77.25
(3) Loss in Bank of Tubes	0.2622	905.25
Total Loss		**990.00**
Enhancement		**154.25**

Table 5: Pressure loss for Case-2: Q_2=67.1936 m^3/s – enhanced design

Losses	**Loss Coefficient**	**Pressure Drop**
	[ ]	[Pa]
(1) Major Loss-Friction	0.0175	8.00
(2) Minor Loss	0.5 and 1.3	84.25
(3) Loss in Bank of Tubes	0.2659	975.5
Total Loss		**1068**
Enhancement		**168.75**

The above pressure loss calculation showed that the proposed enhanced design can reduce the pressure loss across the cooler by 154.25 Pa and 168.75 Pa for Q_1 and Q_2, respectively.

4. TWO DIMENSIONAL COMPUATIONAL MODEL OF THE FLUID FLOW

4. 1 Computational fluid dynamics numerical grid and details

The CFD hardware involves the computer cluster existing in the author's laboratory. It consists of 8 nodes of parallelized computers (2 of the 8 nodes already exist in the UCF laboratory) based on dual AMD 64-bit processors. The software package consists of FLUENT CFD flow solver Version (Version 6.2.16) and Gambit grid generator Version (Version 2.2.30). Numerical details are provided below.

Numerical Grid:

A typical numerical grid for the 2-D numerical model is shown in Figure 5, generated using GAMBIT grid generator [14]. The grid is refined until the maximum difference in pressure at locations of interest is less than 0.2%. The grid details are as follows:

- Grid elements: Quad and hybrid
- Grid type: Map and pave
- Spacing (Interval size) = 4
- Minimum Grid size: Number of cells=125,998.

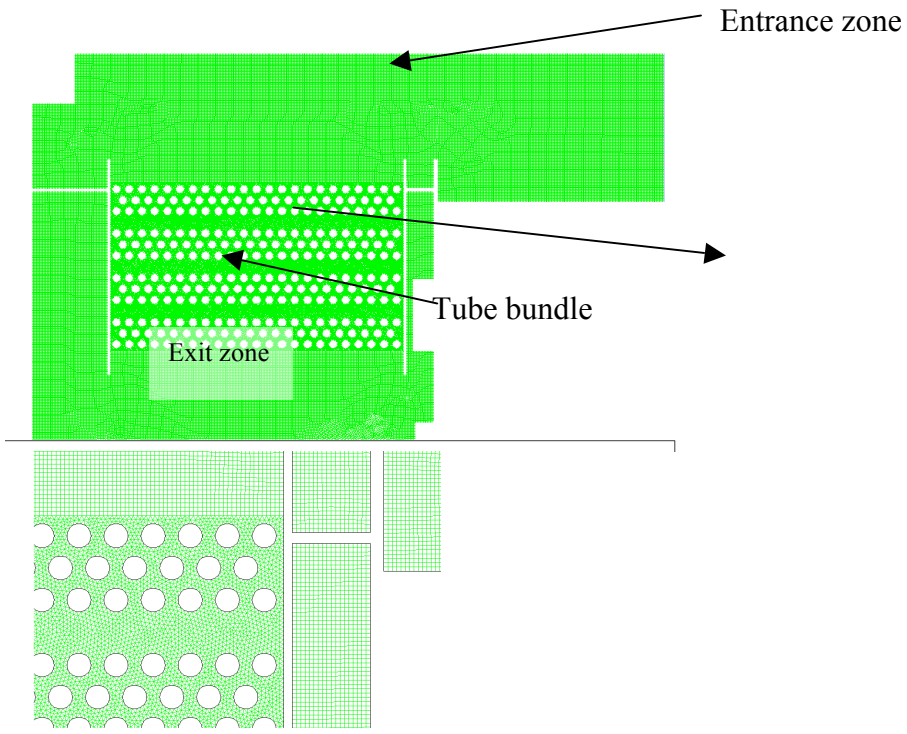

Figure 5: Typical numerical Grid and zones for existing design model

Boundary conditions: At the inlet: Constant mass flow rate in kg/s is applied.
At the exits: Pressure outlet with gage pressure = 0
All other walls: Insulated rough walls with roughness constant =0.5

Turbulence Modeling:

- Model: Realizable k-ε
- Near-wall treatment: Standard wall functions
- Model Constants: C2-Epsilon=1.9, Turbulent Kinetic Energy (TKE) Pr=1, Turbulent Dissipation Rate (TDR) Pr=1.3.

Fluid: Air with constant density= 1.22 kg/m^3. Viscosity is constant=0.000017894 kg/m-s.
Under-relaxation factors for*:* Pressure=0.3, density=1, body forces=1, momentum=0.7, TKE=0.7, TDR=0.7, turbulent viscosity=1.
Descretization: Standard for pressure, SIMPLE for pressure-velocity coupling and second order upwind for momentum, TKE, and TDR.
Convergence*:* Figure 6 below shows the double precision convergence history of the scaled residual for typical case studied. The minimum convergence criteria for the scaled residual of continuity, x-velocity, y-velocity, k and epsilon=1e-12 for all cases studied. The CPU computational time needed to reach convergence for typical case is approximately 20 hours of continuous running time using one processor only.

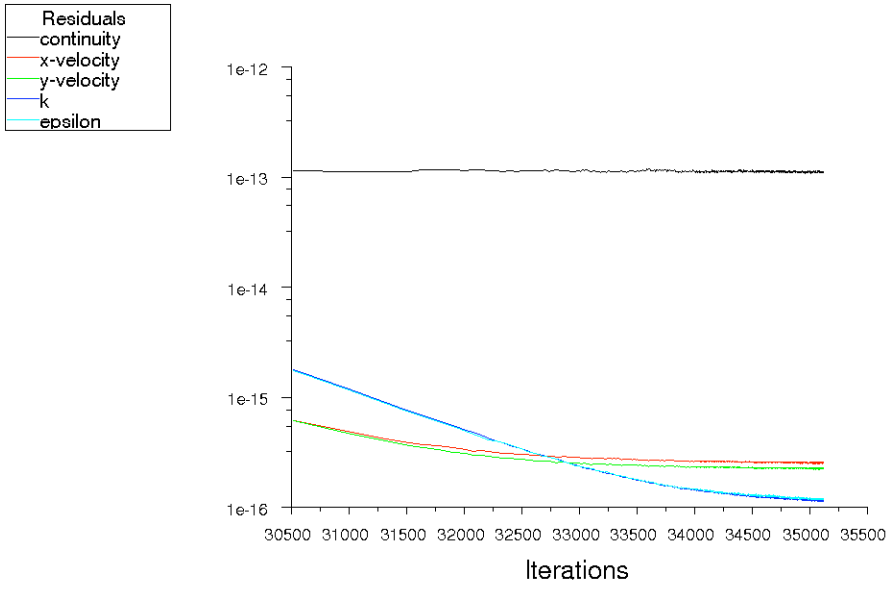

Figure 6: Convergence history

4. 2 Computational fluid dynamics modeling of finned tube bundle

The flow across the bundle with finned tubes is complex and need to be modeled using approaches that are easy to validate with reasonable number of numerical grid points. In this study, two approaches have been investigated to model the tube bundle finned tubes: porous media approximation and effective diameter concept. Discussion of both approaches are provided in the following sections:

4.2.1 Porous media approximation model of the flow across the finned tube bundle

The finned tube bundle is modeled as porous media. Porous media are modeled by the addition of a momentum source term to the standard fluid flow equations. The source term is composed of two parts: a viscous loss term (Darcy, the first term on the right-hand side of Equation 1, and an inertial loss term (the second term on the right-hand side of Equation 1.

$$S_i = -\left(\sum_{j=1}^{3} D_{ij}\mu v_j + \sum_{j=1}^{3} C_{ij}\frac{1}{2}\rho v_{mag} v_j\right) \tag{8}$$

where Si is the source term for the ith (x, y or z) momentum equation, and D and C are prescribed matrices. This momentum sink contributes to the pressure gradient in the porous cell, creating a pressure drop that is proportional to the fluid velocity (or velocity squared) in the cell. To recover the case of simple homogeneous porous media

$$S_i = -\left(\frac{\mu}{\alpha} v_i + C_2\frac{1}{2}\rho v_{mag} v_i\right) \tag{9}$$

where α is the permeability and C2 is the inertial resistance factor.

In laminar flows through porous media, the pressure drop is typically proportional to velocity and the constant C2 can be considered to be zero. Ignoring convective acceleration and diffusion, the porous media model then reduces to Darcy's Law:

$$\nabla p = -\frac{\mu}{\alpha}\vec{v} \tag{10}$$

The pressure drop that the solver computes in each of the two (x, y) coordinate directions within the porous region is then

$$\Delta p_x = \sum_{j=1}^{3} \frac{\mu}{\alpha_{xj}} v_j \Delta n_x \qquad\qquad \Delta p_y = \sum_{j=1}^{3} \frac{\mu}{\alpha_{yj}} v_j \Delta n_y$$

where 1/ αij are the entries in the matrix D in Equation 1, vj are the velocity components in the x and y directions, and Δn_x and Δn_y are the thicknesses of the medium in the x, and y directions. Here, the thickness of the medium (Δn_x and Δn_y) is the *actual* thickness of the porous region in your model.

At high flow velocities, the constant C2 in Equation 9 provides a correction for inertial losses in the porous medium. This constant can be viewed as a loss coefficient per unit length along the flow direction, thereby allowing the pressure drop to be specified as a function of dynamic head. In case of modeling a perforated plate or tube bank, we can sometimes eliminate the permeability term and use the inertial loss term alone, yielding the following simplified form of the porous media equation:

$$\nabla p = -\sum_{j=1}^{3} C_{2_{ij}} \left(\frac{1}{2}\rho v_j v_{mag}\right) \tag{11}$$

The viscous and inertial resistance coefficients are both defined in the same manner. The basic approach for defining the coefficients using a Cartesian coordinate system is to define one direction vector in 2D and then specify the viscous and/or inertial resistance coefficients in each direction. In 2D, the second direction, which is not explicitly defined, is normal to the plane defined by the specified direction vector and the z direction vector.

4.2.1.1 Computational results using porous media approximation

The viscous and inertial coefficients are determined for specified fluid flow rate by tuning these coefficients in the CFD model and the solver is allowed to run and converge until the mass weighted average static pressure drop across the tube bank matched the calculated values using Robinson and Briggs correlations. Results are shown in Table 6.

Table 6

Axial Direction (X)		Radial Direction (Y)		Pressure Drop for	Difference	Pressure Drop for	Difference
D	C	D	C	Q1		Q2	
1/m^2	1/m	1/m^2	1/m	in H2O	%	in H2O	%
30	85	2	7	3.678	0.75	4.004	0.60

Pressure distribution across the flow domain including the tube bundle is shown in Figure 7 and velocity vectors are shown by Figure 8 below. All results provided below are for flow rate of Q_2. The pressure and velocity distributions in the entrance zone are not uniform as shown by Figures 7 and 8 especially at the corners where the flow changes direction. As a result, the pressure distribution across the tube bundle is not uniform as well.

The disadvantages of the porous media approximation approach are that:

- The viscous and inertial coefficients, D, and C coefficients need to be tuned for every individual case, a process that requires large amount of computational time. In addition, validation of these coefficients depends on the availability of experimental data for every single case, which are not available.
- It is not possible to have actual velocity field distribution (velocity vectors and magnitudes) across the tube bundle. This fact makes it impossible to track the fluid path across the tube bundle.

Because of these disadvantages, the author used the second approach, the effective diameter concept, which is addressed next.

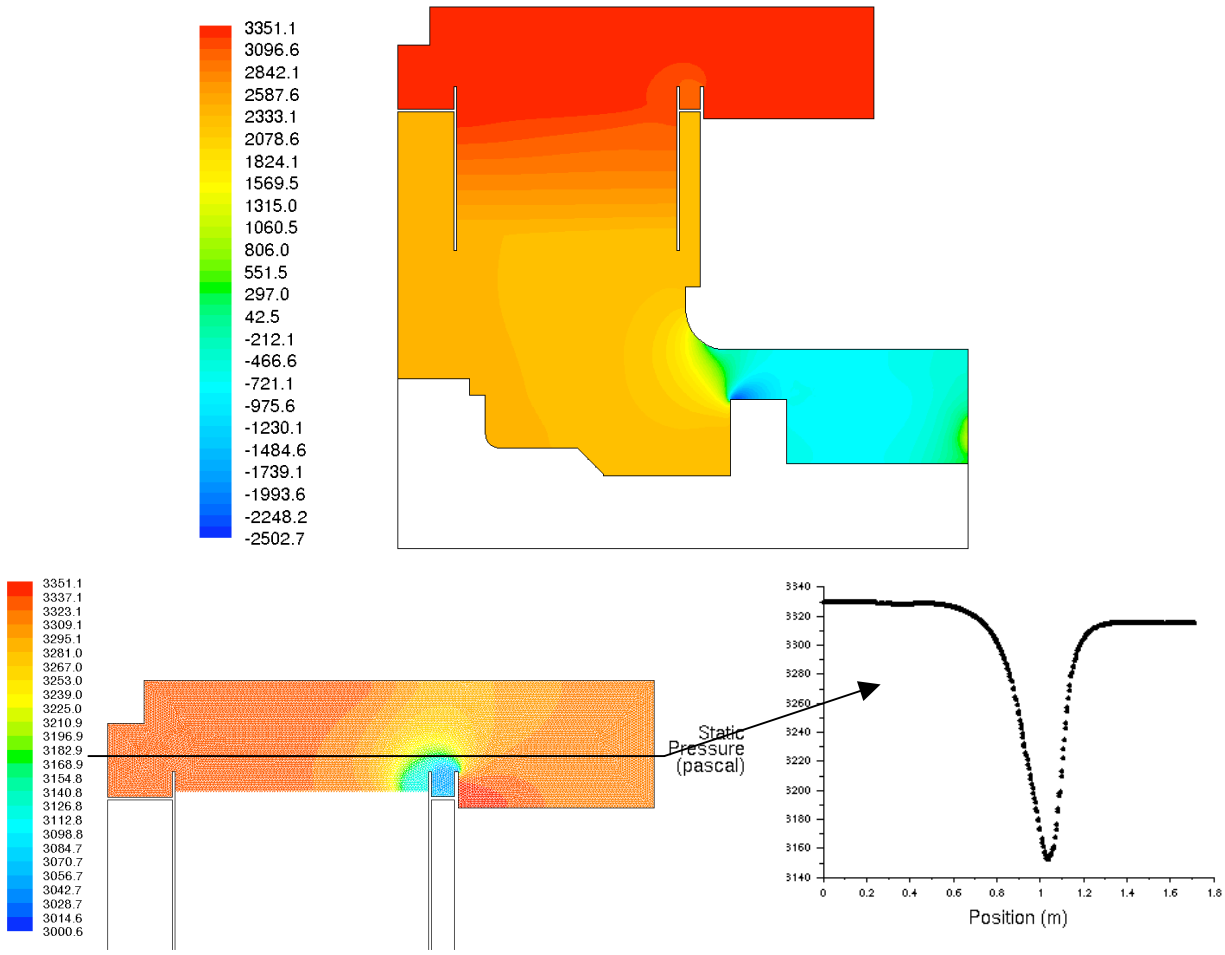

Figure 7: Pressure distribution (in Pa) on the inlet and the tube bundle for existing geometry using porous media modeling approach

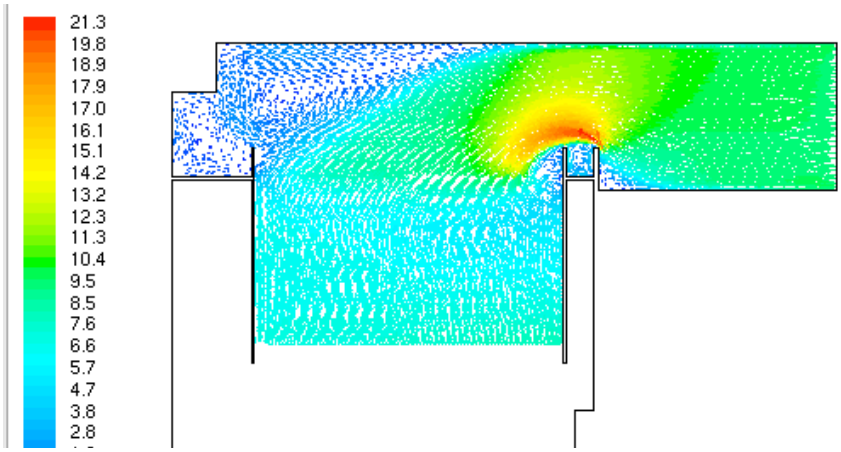

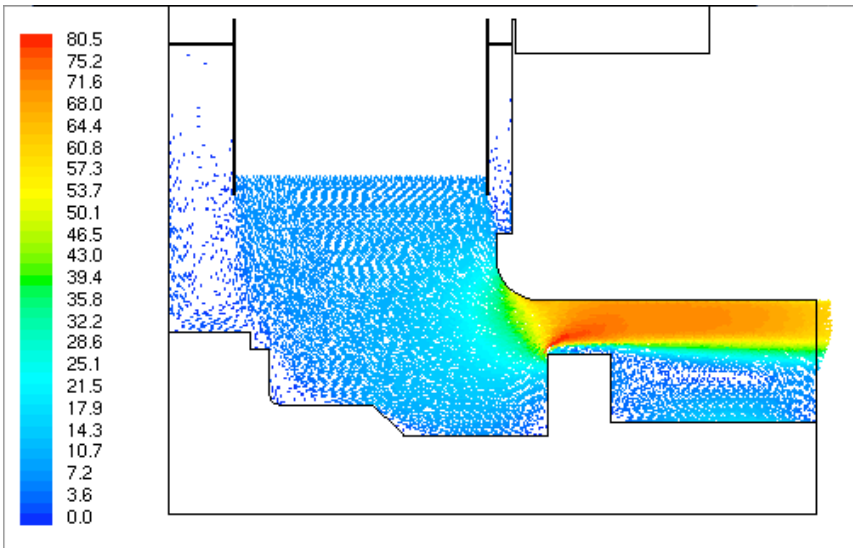

Figure 8: Velocity vectors (in m/s) on the inlet and the tube bundle for existing geometry using porous media modeling approach

4.2.2 Effective Diameter Concept:

4.2.2.1 Definition and advantages

The finned tubes are modeled using the effective diameter concept. The effective diameter is defined as the diameter of the tubes without fins that would provide the same pressure drop as that for finned tubes. The advantage of this approach over the porous media approximation is that the path of the fluid and the detailed history of the pressure and velocity across the tube bundle can be tracked. To demonstrate this advantage, velocity vectors and pressure distribution results are provided by Figures 9 and 10 below for an assumed tube effective diameter of 30mm as starting point to study the flow patterns for fluid flow rate of Q_2(actual).

The pressure distribution along a horizontal path after each row of tubes is shown in Figure 10 where the variation in static pressure magnitudes from left to right sides of the tube bundle can be calculated precisely. Hence the effective diameter approach will be used to model the flow across the tube bundle.

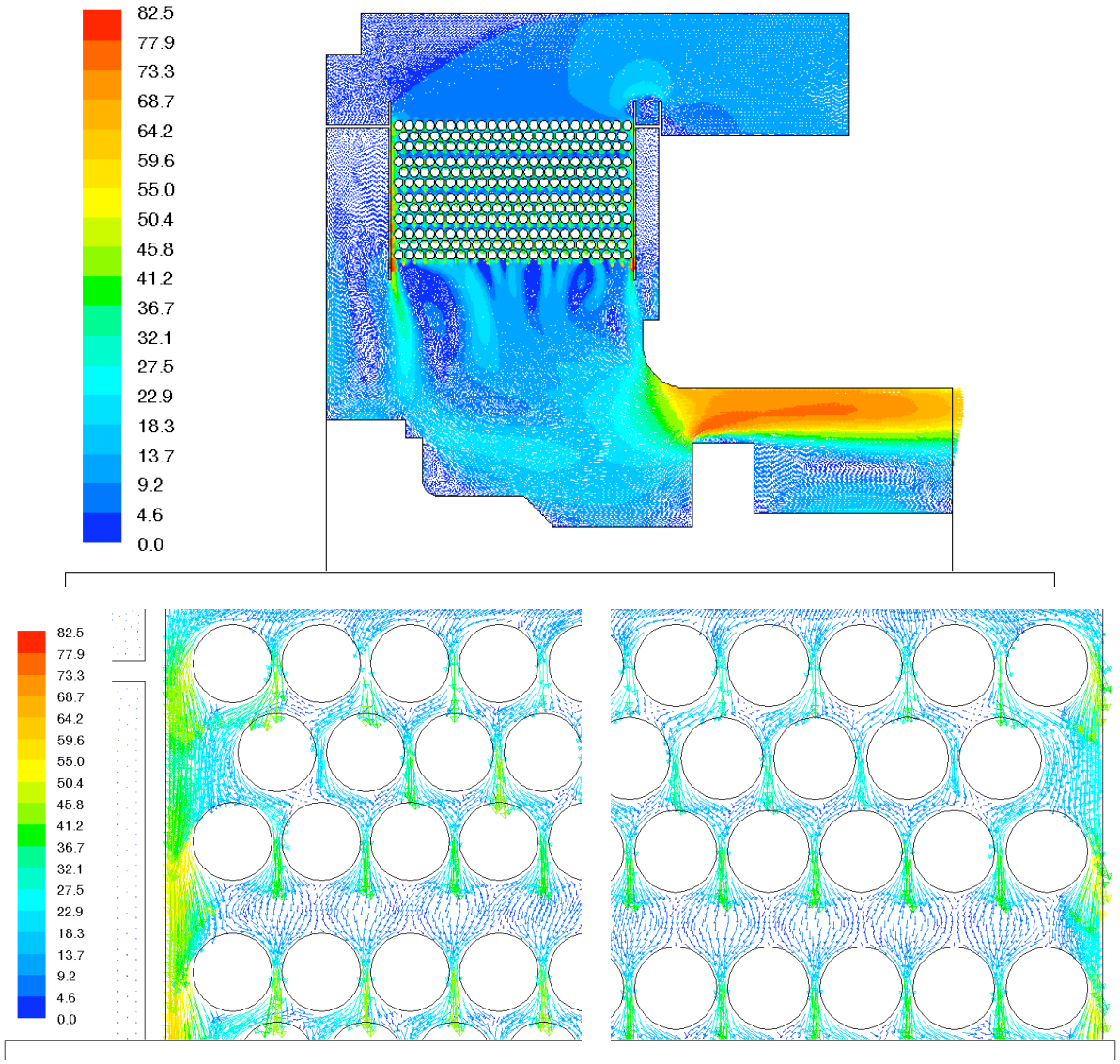

Figure 9: Velocity vectors (in m/s) distribution using effective diameter approach for an assumed tube effective diameter of 30 mm and Q2(actual). (For demonstration purposes)

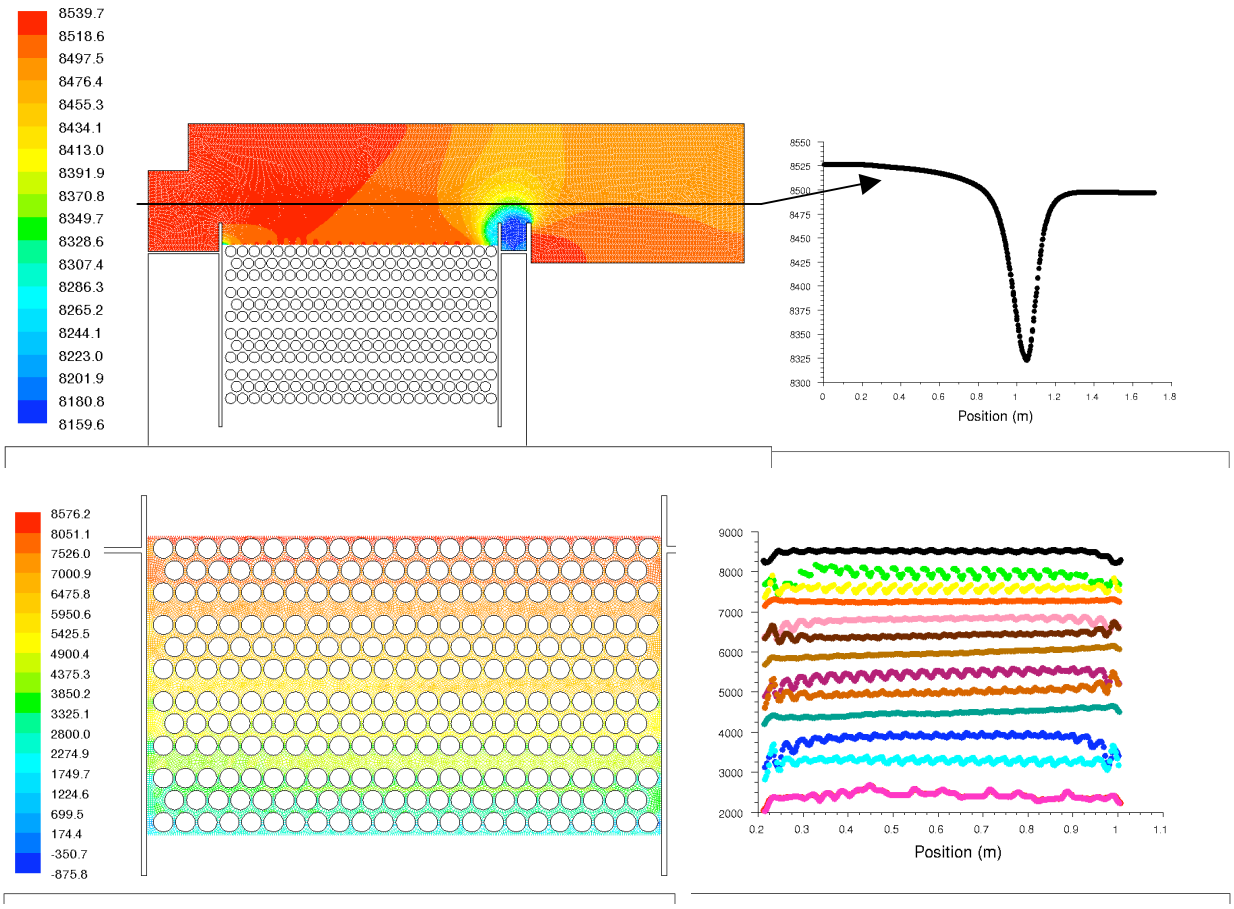

Figure 10: Static pressure (in Pa) distribution using effective diameter approach for an assumed tube effective diameter of 30 mm and Q2(actual). (For demonstration purposes)

4.2.2.2 Effective diameter determination based on experimental test and geometry

The concept of effective diameter is validated by tuning the diameter of the tubes and comparing the resulting pressure drop with experimental data for tested geometry with finned tubes. Results provided here are determined based on investigation carried out for three cases of tubes diameter=20mm, 22.5mm and 25mm over a range of flow rate. Geometry # 0 is used for this particular study as this geometry matches the experimental rig geometry. Investigation of pressure drop with tubes of 22.5mm diameter showed that the agreement with corresponding experimental pressure drop data is to within less than 1% at operational flow rates (see Figure 11). Hence, it is determined that tubes with 22.5mm diameter (the effective diameter) with no fins would provide the same pressure drop as finned tubes with 20mm tube diameter and 3mm fin pitch.

Figure 12 shows typical velocity vectors and pressure distribution results for the highest volume flow rate tested of 35 m3/s.

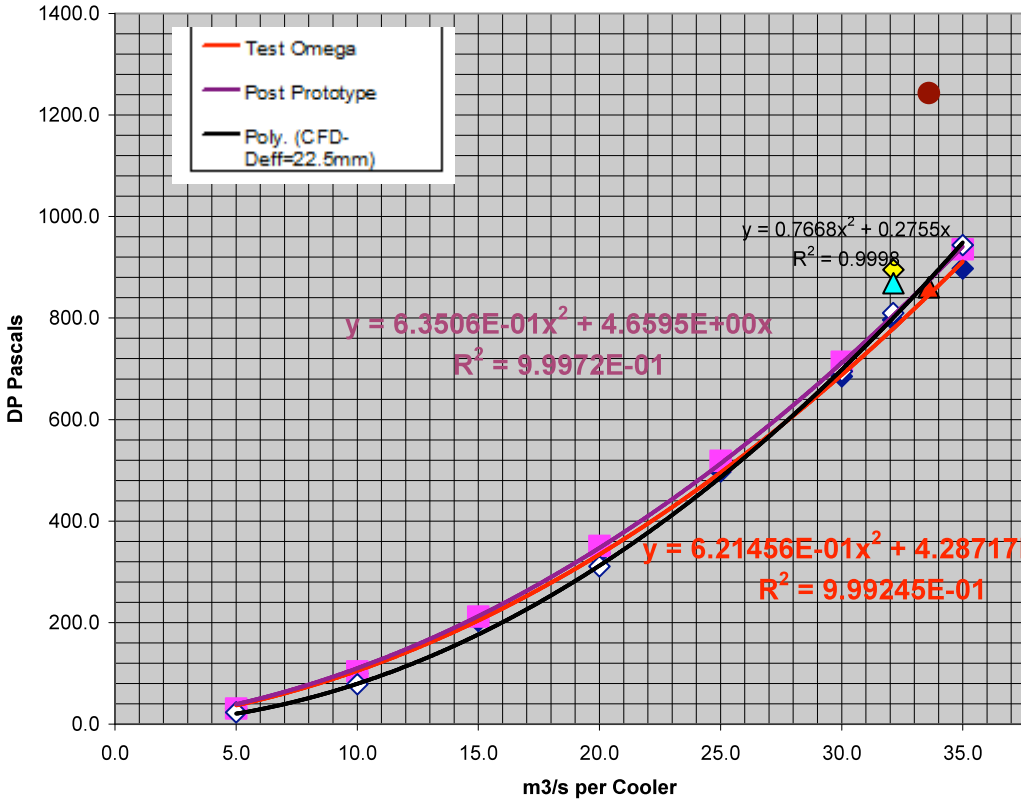

Figure 11: Experimental Data: Pressure drop versus flow rate to determine the effective tube diameter

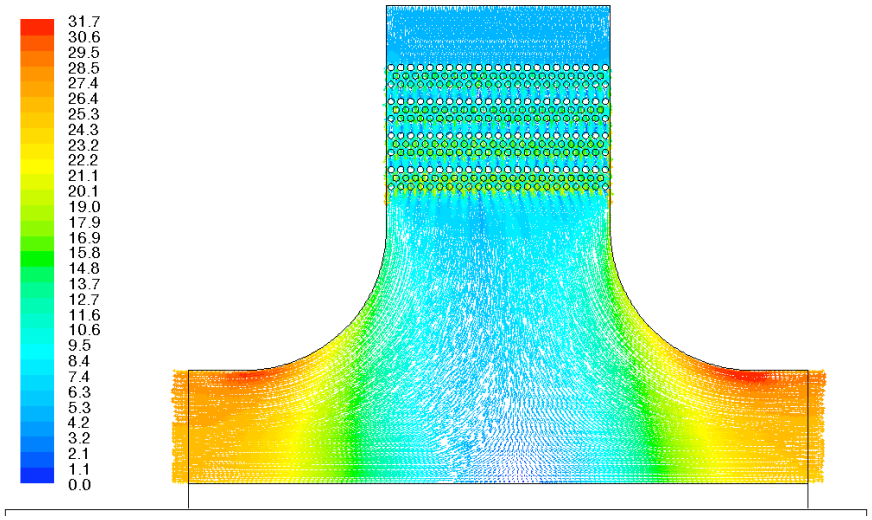

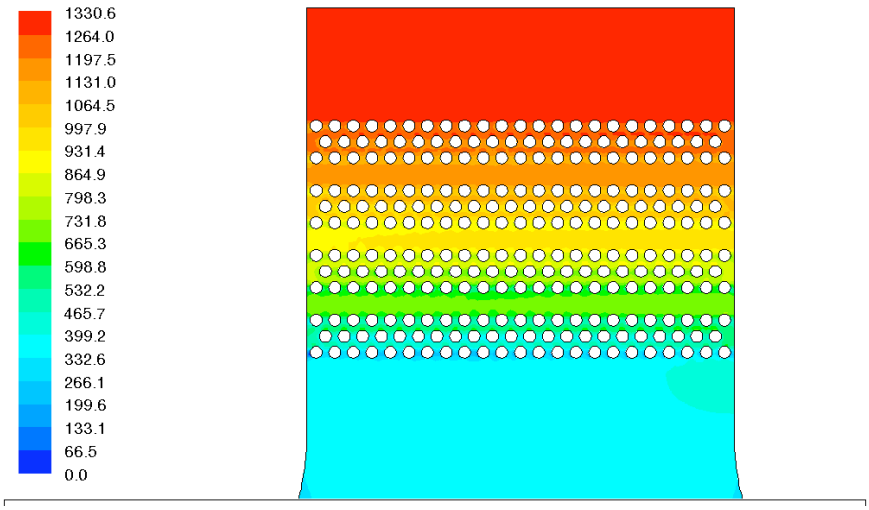

Figure 12: Velocity vectors (in m/s) and pressure distribution results for the highest volume flow rate of 35 m3/s. (Geometry # 0)

4.2.2.3 Pressure drop for existing geometry based on effective diameter

The finned tubes are modeled using the effective diameter concept. The effective diameter is 22.5mm as shown above. CFD simulations for existing flow geometry (Geometry #1) with finned tubes modeled using the determined effective diameter of 22.5mm showed that the mass weighted average pressure drop across the tube bundle= 1066.5 Pa = 4.29 in H_2O for the highest volume flow rate of 35 m3/s compared to 944 Pa=3.87 in H_2O for the straight inlet case (Geometry # 0) and for the same flow rate. Figure 13 shows pressure distribution on the entrance and across tube bundle zones, pressure distribution along the inlet and the exit of the tube bundle and velocity vectors distribution. It is clearly shown that the pressure distribution along each row of tubes is not uniform because of the inlet geometry.

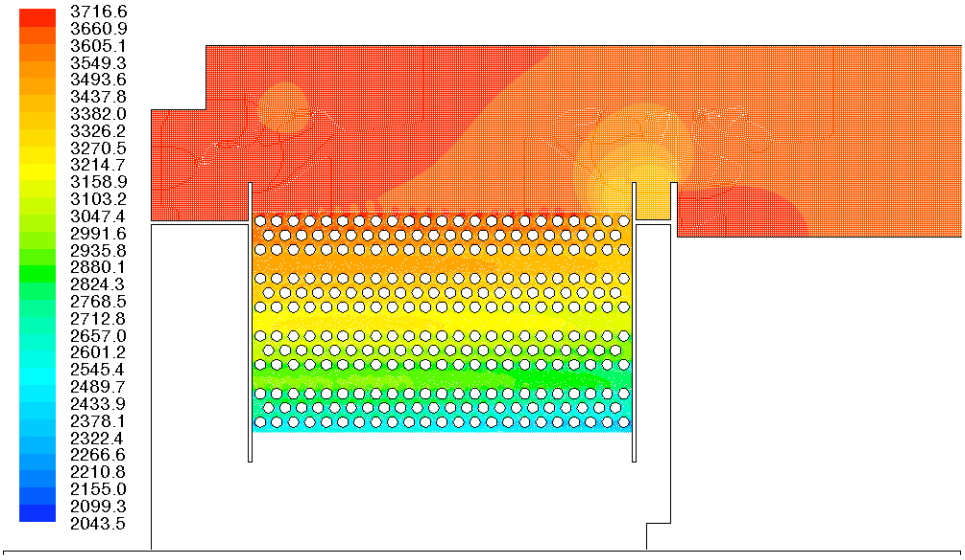

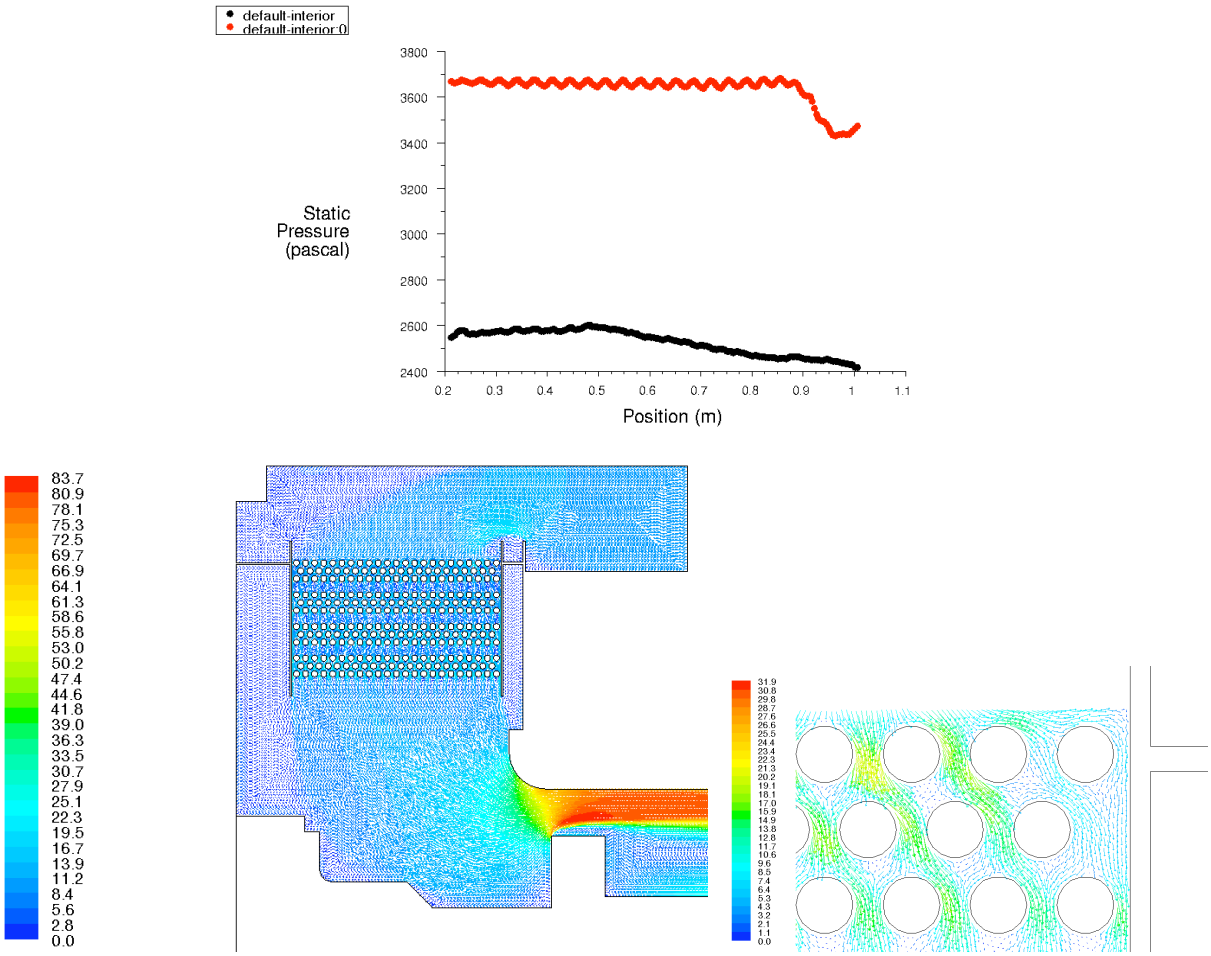

Figure 13: Pressure distribution (in Pa) on the entrance and across tube bundle zones, pressure distribution along the inlet and the exit of the tube bundle and velocity vectors distribution for Q=35 m3/s

4.2.2.4 Pressure drop for enhanced geometries based on effective diameter

The main goal of this study is to reduce the pressure drop across the cooler and to use that reduction in pressure drop to enhance the performance of the cooler by introducing more dense finned tubes of fin pitch = 3.0mm instead of 3.5 mm pitch that is being used at present. With this goal in mind, several enhancements on the inlet zone of the cooler is proposed and CFD model for each geometry is built and pressure drop results for each geometry is compared to pressure drop results of the existing geometry (Geometry #1). Figure 14 shows the velocity vectors and pressure distribution for each investigated geometry at flow rate = 35 m^3/s. Summary of the corresponding mass weighted pressure drop for each geometry between two different locations is given in Table 7. The pressure drop reduction associated with each geometry compared to the existing geometry is listed in Table 7 as well

Pressure drop (1-1) is the mass weighted average pressure at the tube bundle inlet minus the mass weighted average pressure at the tube bundle exit.

Pressure drop (2-2) is the mass weighted average pressure at the inlet of the cooler minus the mass weighted average pressure at the tube bundle exit.

4.2.2.5 Overall conclusion

The following can be concluded based on the above discussion:

- Geometry # 7 showed that 185 Pa in pressure drop can be saved (16% enhancement) compared to pressure drop found in existing geometry # 1. Geometry # 7 is achieved by replacing the 90 deg sharp turn by a rounded turn with 600 mm fillet.
- Altering the existing geometry from the right side of the tube bundle shown in Figure 14, did not lead to any reduction in total pressure drop.
- The saved 185 Pa pressure reduction can be used to enhance the overall performance of the cooler introducing more dense finned tubes of fin pitch = 3.0 mm instead of 3.5mm pitch that is being used at present.

4.2.2.4 Effective diameters of finned tube bundle with fin pitch = 3mm

Three cases plotted in Figure 15 are studied to determine the effective diameter of the case with fins pitch =3 mm. Tubes with 20mm, 22.5 mm and 25mm are studied for pressure drop at flow rate of Q2 = 33.6 m^3/s. Based on pressure drop given by Figure 15 and compared to experimental pressure drop for 3mm fin pitch, the tube effective diameter that corresponds to this pressure drop is 23.7mm.

Existing Geometry (Geometry #1)

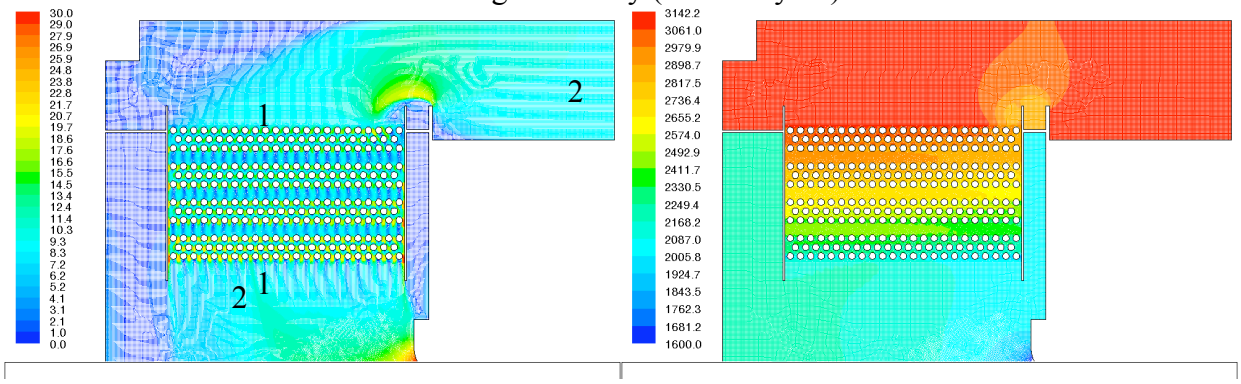

(Geometry #2) - 200 mm fillet

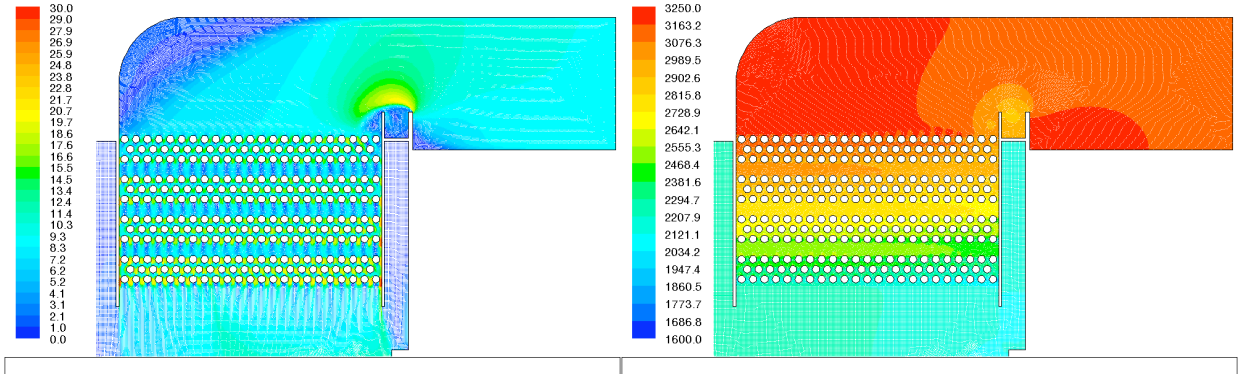

(Geometry # 3) 300 mm fillet

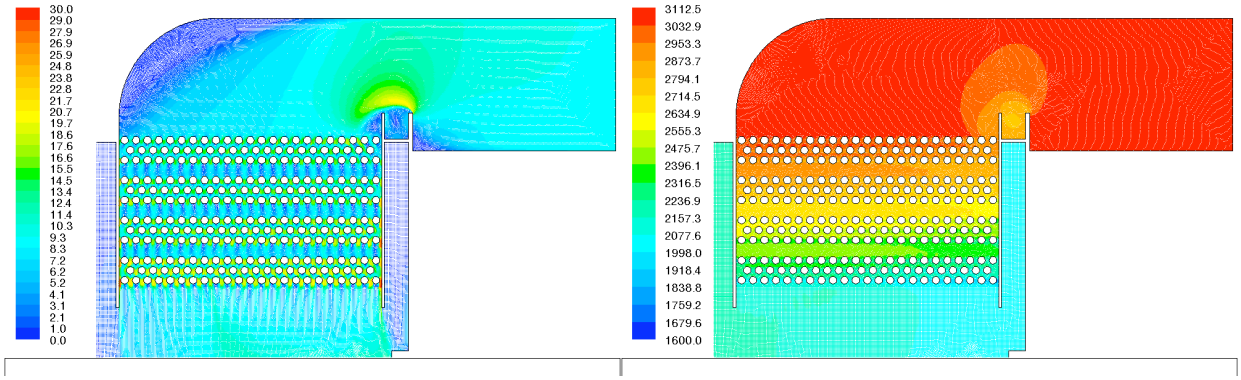

(Geometry # 4) 300 mm fillet and right side modification 1

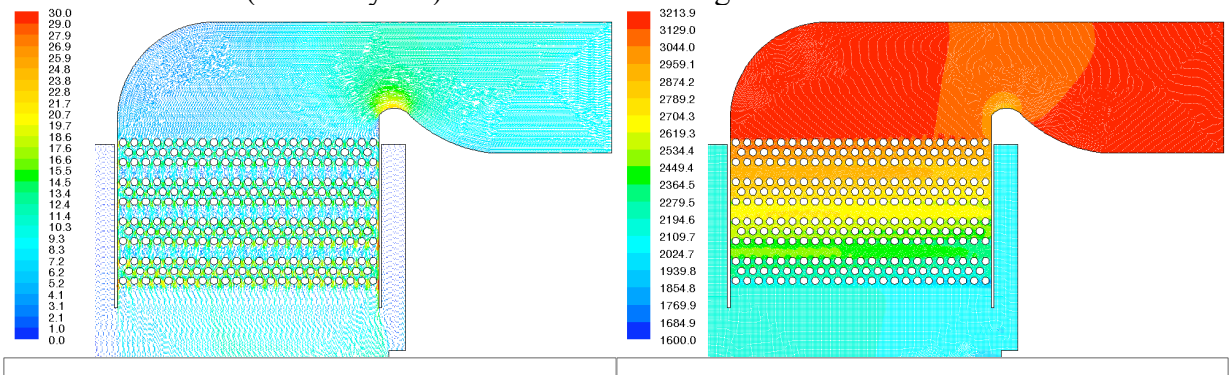

(Geometry # 5) 600 mm fillet

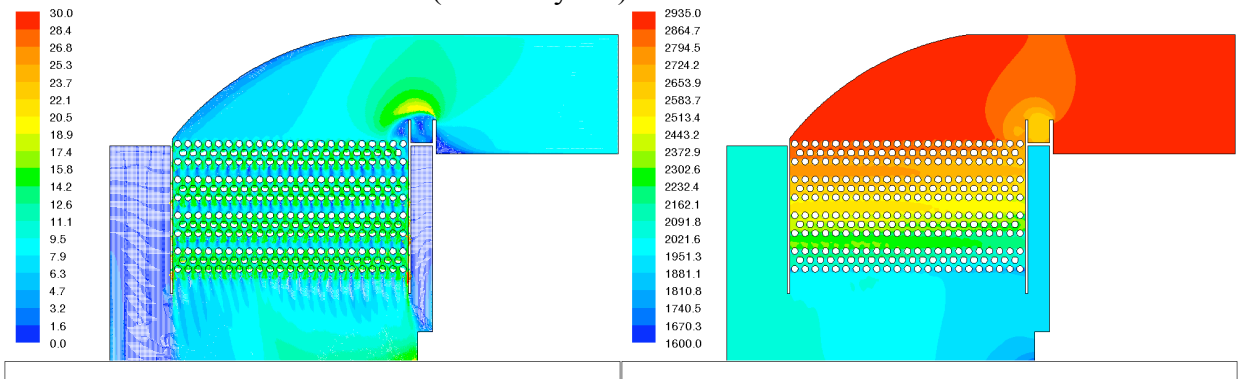

(Geometry # 6) 600 mm fillet and right side modification 2

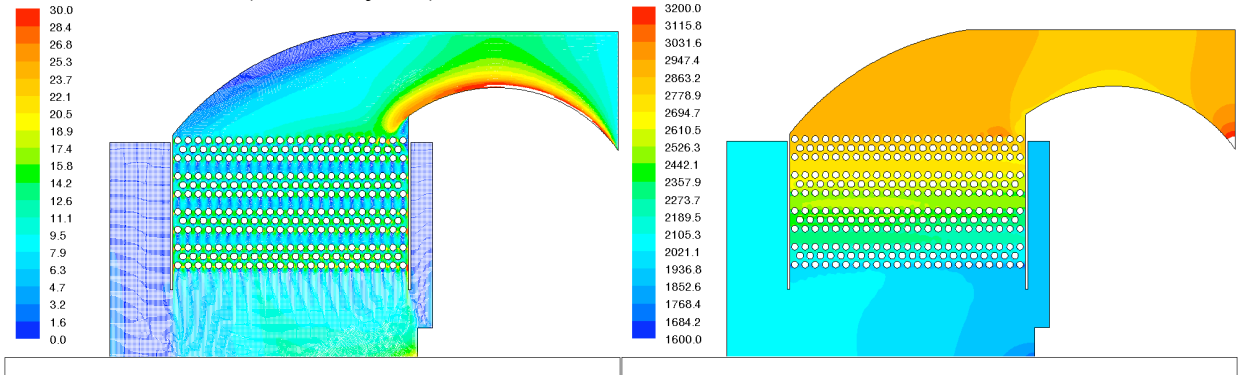

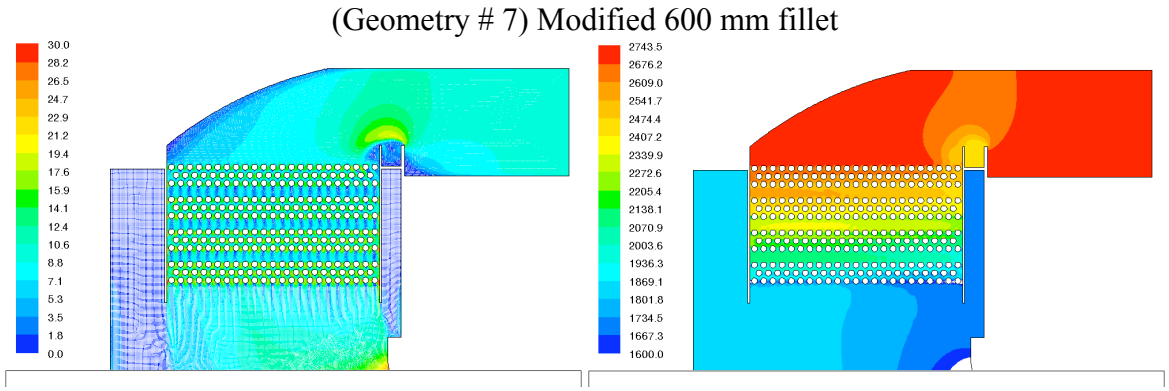

Figure 14 Velocity vectors (in m/s) and pressure distribution (in Pa) for each proposed geometry compared to existing geometry at flow rate = 35 m^3/s.

Table 7: Summary of mass weighted average pressure drop for each geometry between two locations: 1-1 and 2-2 at flow rate = 35 m^3/s

	Static Pressure drop (1-1)		**Total Pressure drop (1-1)**	
	Pa	in H2O	Pa	in H2O
Geometry # 1. Existing Geometry	1066.50	4.29	1046.49	4.21
Geometry # 2 with 200 mm fillet	967.00	3.89	945.00	3.80
Saved	99.50	0.40	101.49	0.41
Geometry # 3 with 300 mm fillet	967.50	3.89	943.95	3.79
Saved	99.00	0.40	102.54	0.41
Geometry # 4 with 300 mm fillet	1038.34	4.17	1002.10	4.03
Saved	28.16	0.11	44.39	0.18
Geometry # 5	924.15	3.71	902.00	3.63
Saved	142.35	0.57	144.49	0.58
Geometry # 6	935.69	3.76	954.77	3.84
Saved	130.81	0.53	91.72	0.37
Geometry # 7	925.35	3.72	902.85	3.63
Saved	141.15	0.57	143.64	0.58

	Static Pressure drop (2-2)		**Total Pressure drop (2-2)**	
	Pa	in H2O	Pa	in H2O
Geometry # 1. Existing Geometry	1109.16	4.46	1093.58	4.40
Geometry # 2 with 200 mm fillet	968.50	3.89	958.10	3.85
Saved	140.66	0.57	135.48	0.54
Geometry # 3 with 300 mm fillet	967.60	3.89	957.00	3.85
Saved	141.56	0.57	136.58	0.55
Geometry # 4 with 300 mm fillet	1038.20	4.17	1028.00	4.13
Saved	70.96	0.29	65.58	0.26
Geometry # 5	925.30	3.72	915.30	3.68
Saved	183.86	0.74	178.28	0.72
Geometry # 6	1016.00	4.08	1008.44	4.05
Saved	93.16	0.37	85.14	0.34
Geometry # 7	925.48	3.72	916.00	3.68
Saved	183.68	0.74	177.58	0.71

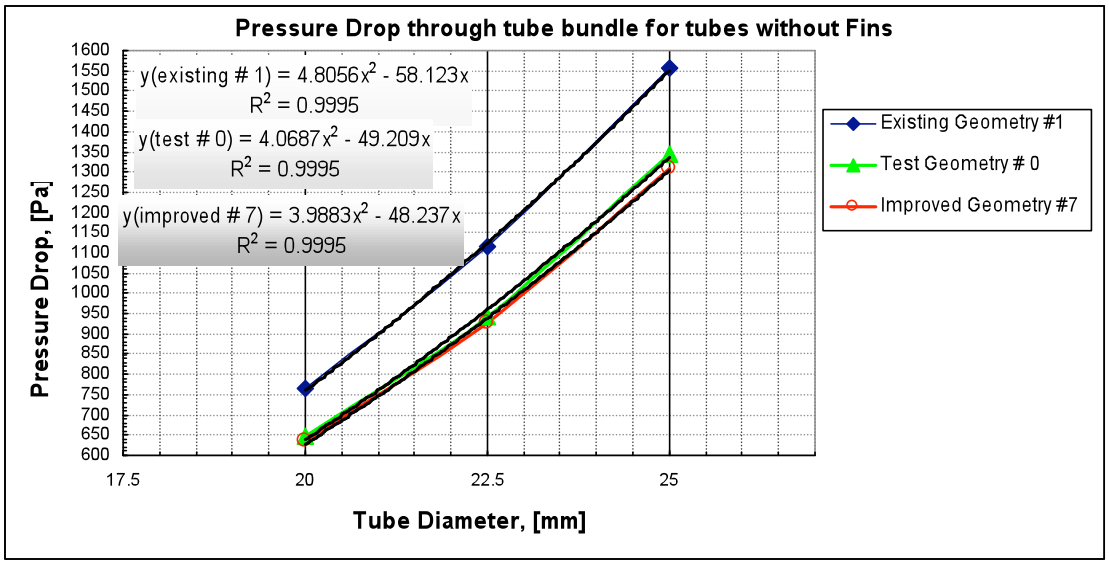

Figure 15: Pressure drop for tubes with 20mm, 22.5 mm and 25mm at flow rate of Q2 = 33.6 m^3/s.

5. REFERENCES

[1] Lee, Y. N. and Minkowycz, W. J., "Heat Transfer Characteristics of the Annulus of Two Coaxial Cylinders With One Cylinder Rotating," *Int. J. Heat Mass Transf.*, pp. 711-722, 1989.

[2] Hayase, T., Humphrey, J. A. C., and Greif, R., "Numerical Calculations of Convective Heat Transfer Between Rotating Coaxial Cylinders With Periodically Embedded Cavities," *ASME J. Heat Transfer*, vol. 114, pp. 589-596, 1992.

[3] Sommerer, Y. and Lauriat, G., "Numerical Study of Steady Forced Convection in a Grooved Annulus Using a Design of Experiments," *ASME J. Heat Transfer*, vol. 123, pp. 837-848, 2001.

[4] Institution of Mechanical Engineers (Great Britain).Thermodynamics and Fluid Mechanics, Heat transfer and fluid flow in electrical machines: a symposium arranged by the Thermodynamics and Fluid Mechanics Group, 23rd October 1969. London: Institution of Mechanical Engineers, 1970.

[5] A. K. Sleiti and J. S. Kapat, 2006 " Heat Transfer in Channels in Parallel-Mode Rotating at High Rotation Numbers ", AIAA Journal of Thermophysics and Heat Transfer, Vol. 20, No.4, pp. 748-753, October-December 2006.

[6] A. K. Sleiti and J. S. Kapat, 2005, " Fluid Flow and Heat Transfer in Rotating Curved Duct at High Rotation and Density Ratios ", ASME Journal of Turbomachinery, Volume 127, Issue 4, pp. 659-667.

[7] A. K. Sleiti and J. S. Kapat, 2006 "*An Experimental Investigation of Liquid Jet Array and Single Phase Spray Impingement Cooling Using Polyalphaolefin*", Experimental Heat Transfer Journal, Volume 19, No. 2, pp. 149-163 April 2006.

[8] A. K. Sleiti and J. S. Kapat, 2006, "Effect *of Coriolis and Centrifugal Forces at High Rotation and Density Ratios*", AIAA Journal of Thermophysics and Heat Transfer), Volume 20, No. 1, pp. 67-79.

[9] A. K. Sleiti , 2007, "Advanced cooling technology for rotors of high-power low-duty cycle generators using polyalphaolefins" Journal of Synthetic Lubrication, Vol. 24, No.2, pp. 77-90, March 2007.

[10] F. P. Incropera and D. P. Dewitt, *Fundamentals of Heat and Mass Transfer*, John Wiley, New York, 2002.

[11] Kays, W.M., and A.L. London, 1984. *Compact Heat Exchangers*, 3rd ed., McGraw-Hill, New York.

[12] J. Stasiulevicius and A. Skrinska, 1988. *Heat Transfer of Finned Tube Bundles in Crossflow,* Hemisphere Publication Corporation, New York.

[13] Robinson, K.K. and Briggs, D.E. 1966. Pressure Drop of Air Flowing Across Triangular Pitch Banks of Finned Tubes, Chem. Engng. Prog. Sym. Series, 62(64): 177-184.

[14] Fluent 6.2 Reference Manual